Giant Thermal Enhancement of the Electric Polarization in Ferrimagnetic $BiFe_{1-x}Co_xO_3$ Solid Solutions near Room Temperature

César Menéndez[1] and Claudio Cazorla[2]
[1]School of Materials Science and Engineering, UNSW Sydney, Sydney, New South Wales 2052, Australia
[2]Departament de Física, Universitat Politècnica de Catalunya, Campus Nord B4-B5, E-08034 Barcelona, Spain

(Received 5 March 2020; accepted 20 August 2020; published 9 September 2020)

Thermal excitations typically reduce the electric polarization in ferroelectric materials. Here, we show by means of first-principles calculations that multiferroic $BiFe_{1-x}Co_xO_3$ solid solutions with $0.25 \leq x \leq 0.50$ (BFCO) represent a noteworthy exception to this behavior. In particular, we find that, at room temperature and for moderate pressures of 0.1–1.0 GPa, depending on the composition, the electric polarization of bulk BFCO increases by ∼150%. The origin of such an exceptional behavior is a phase transformation involving a low-T rhombohedral ($\mathcal{R}$) phase and a high-T supertetragonal ($\mathcal{T}$) phase. Both $\mathcal{R}$ and $\mathcal{T}$ phases are ferrimagnetic near room temperature with an approximate net magnetization of 0.13 μ_B per formula unit. Contrary to what occurs in either bulk $BiFeO_3$ or $BiCoO_3$, the $\mathcal{T}$ phase is stabilized over the $\mathcal{R}$ by increasing temperature due to its higher vibrational entropy. This extraordinary T-induced $\mathcal{R} \rightarrow \mathcal{T}$ phase transition is originated by polar phonon modes that involve concerted displacements of transition-metal and oxygen ions.

DOI: 10.1103/PhysRevLett.125.117601

Supertetragonal ($\mathcal{T}$) oxide perovskites comprise a family of materials that are fundamentally intriguing and have great potential for ferroelectric, piezoelectric, sensing, and energy conversion applications [1–3]. Supertetragonal phases exhibit giant electric polarizations on the order of 100 $\mu C/cm^2$ and may be accompanied by magnetism [4–6]. The coexistence of ferroelectricity and magnetism in crystals, known as multiferroics, offers the possibility of controlling the magnetization with electric fields via their cross-order coupling. Magnetoelectric couplings can be used, for example, to design ultraefficient logic and memory devices and realize large piezomagnetic coefficients for the miniaturization of antennas and sensors [7–10]. Furthermore, phase transitions involving $\mathcal{T}$ phases typically exhibit colossal volume changes of ∼10% (e.g., $PbVO_3$ and related solid solutions), which can be exploited in mechanical degradation [11,12] and solid-state cooling [13–15] applications. Examples of $\mathcal{T}$ multiferroic materials are bulk $BiCoO_3$ (BCO) and $BiFeO_3$ (BFO) thin films [16–18].

Nonetheless, $\mathcal{T}$ phases usually are thermodynamically too stable and hence difficult to switch by means of an external field or temperature, which severely limits their technological applicability. For example, in order to stabilize a paraelectric phase in multiferroic $\mathcal{T}$ $BiCoO_3$, it is necessary to increase its temperature above 800 K or apply a large hydrostatic pressure of $P > 3$ GPa [19–21]. Likewise, the functionality of supertetragonal $BiFeO_3$ thin films only can be exploited within a narrow epitaxial strain interval in which the $\mathcal{T}$ phase coexists with other polymorphs and consequently becomes structurally soft [22,23]. Moreover, $\mathcal{T}$ multiferroics mostly are antiferromagnetic (i.e., their atomic magnetic moments align antiparallel, rendering negligible net magnetizations) and consequently are unresponsive to external magnetic fields [24]. Therefore, it is highly desirable to find new $\mathcal{T}$ multiferroic materials that react significantly to external bias near ambient conditions.

In this Letter, we show by means of first-principles calculations based on density functional theory (DFT) that $BiFe_{1-x}Co_xO_3$ solid solutions (BFCO) with $0.25 \leq x \leq 0.50$ represent ideal bulk systems in which to realize the full potential of multiferroic $\mathcal{T}$ phases. Specifically, we find that, under moderate hydrostatic pressures of $0.1 \lesssim P \lesssim 1$ GPa (depending on the composition), it is possible to trigger a phase transition from a low-T rhombohedral ($\mathcal{R}$) phase to a high-T $\mathcal{T}$ phase at room temperature. The disclosed T-induced $\mathcal{R} \rightarrow \mathcal{T}$ phase transformation involves (i) a colossal increase in the electric polarization of $\Delta p \sim 150\%$, (ii) the existence of a robust net magnetization of ≈ 0.13 μ_B per formula unit (f.u.), and (iii) a giant volume increase of $\Delta V \sim 10\%$. Examples of technologies in which these multifunctional phenomena could have an impact include pyroelectric energy harvesting [25,26] and solid-state cooling [27]. Meanwhile, the appearance of ferrimagnetism and the stabilization of the $\mathcal{T}$ phase over the $\mathcal{R}$ with increasing temperature, effects that are both missing in bulk $BiCoO_3$ and $BiFeO_3$, pose a series of interesting fundamental questions: Which atomistic mechanisms are responsible for such an anomalous $dp/dT \gg 0$ behavior? What type of thermal excitations drive the uncovered $\mathcal{R} \rightarrow \mathcal{T}$ transformation? Why does Co-Fe cation mixing

trigger a net magnetization in bulk BFCO? Based on our DFT outcomes and analysis, we address these compelling questions and make insightful connections with the experimental results recently reported for $BiFe_{1-x}Co_xO_3$ solid solutions [28–30].

Spin-polarized DFT calculations were performed with the generalized gradient approximation proposed by Perdew *et al.* (PBE) [31] and the range-separated hybrid functional introduced by Heyd *et al.* (HSE06) [32] as implemented in the VASP package [33]. The "Hubbard-U" scheme due to Dudarev *et al.* was employed in the PBE calculations for treating better the Co (Fe) $3d$ electrons, adopting a U value of 6 (4) eV [20,21,34]. The "projected augmented wave" method [35] was used to represent the ionic cores considering the following electronic states as valence: Co $4s^1 3d^8$, Fe $3p^6 4s^1 3d^7$, Bi $6s^2 5d^{10} 6p^3$, and O $2s^2 2p^4$. An energy cutoff of 800 eV and a Γ-centered **k**-point grid of $4 \times 6 \times 6$ were employed for a $2 \times \sqrt{2} \times \sqrt{2}$ simulation cell containing 20 atoms [36], thus obtaining zero-temperature energies converged to within 0.5 meV/f.u. Geometry relaxations were performed for an atomic force threshold of 0.005 eV $Å^{-1}$. Electric polarizations were accurately estimated with the hybrid HSE06 functional and the Berry phase formalism [37–39] (for comparison purposes, we also calculated approximate electric polarizations with the Born effective charges approach [36], Supplemental Material [40]). *Ab initio* free energies were estimated within the quasiharmonic (QH) approximation [34,43] as a function of P and T. Phonon frequencies were calculated with the small displacement method [44,45]. The following technical parameters provided QH free energies converged to within 5 meV/f.u.: 160-atom supercells, atomic displacements of 0.01 Å, and q-point grids of $16 \times 16 \times 16$ for integration within the first Brillouin zone. The effects of chemical disorder were addressed by generating all possible atomic Co-Fe and magnetic spin arrangements (FM and AFM of type A, C, and G; Supplemental Material, Fig. 1 [40]) for a $2 \times 2\sqrt{2} \times \sqrt{2}$ supercell containing 40 atoms. Quasiharmonic free energies were calculated only for the lowest-energy configurations. Our spin-polarized DFT calculations were performed for bulk $BiFe_{0.5}Co_{0.5}O_3$ and $BiFe_{0.75}Co_{0.25}O_3$, hereafter referred to as $BFCO_{0.5}$ and $BFCO_{0.25}$.

Following a previous work by Diéguez and Íñiguez [46], we considered the four $BFCO_{0.5}$ crystal structures that are energetically most competitive at zero temperature. The crystal symmetry of such phases prior to introducing chemical disorder on the metal cation sites were tetragonal ($P4mm$), orthorhombic ($Pnma$), monoclinic (Pc), and rhombohedral ($R3c$). The optimized $BFCO_{0.5}$ structures resulting from such parent phases were labeled as $\mathcal{T}$, $\mathcal{O}$, $\mathcal{M}$, and $\mathcal{R}$, respectively (Supplemental Material, Fig. 1 [40]). Initially, a 20-atom unit cell was employed to model all four polymorphs and to determine the atomic Co-Fe and magnetic spin arrangements (FM and AFM of type A, C, and G; Supplemental Material, Fig. 1 [40]) that render the lowest energies (Fig. 1). In addition, we considered a recently reported orthorhombic phase that exhibits complex and nanotwinned O_6 tilting patterns [47] and which requires a larger simulation cell (Supplemental Material, Fig. 2 [40]).

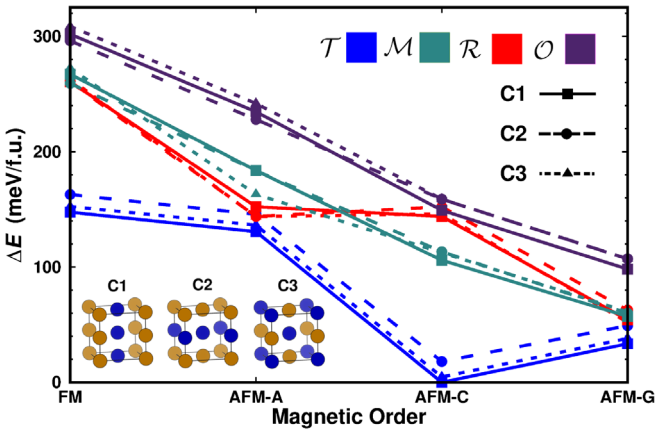

FIG. 1. First-principles analysis of bulk $BiFe_{0.5}Co_{0.5}O_3$ at zero pressure and $T = 0$. Crystal structures with tetragonal ($\mathcal{T}$), monoclinic ($\mathcal{M}$), rhombohedral ($\mathcal{R}$), and orthorhombic ($\mathcal{O}$) symmetry were considered (Supplemental Material, Fig. 1 [40]). All possible Co-Fe (C1, C2, and C3) and magnetic spin arrangements [ferromagnetic (FM) and antiferromagnetic (AFM) of type A, C, and G; Supplemental Material, Fig. 1 [40]] were generated for a $2 \times \sqrt{2} \times \sqrt{2}$ simulation cell containing 20 atoms [36].

The $BFCO_{0.5}$ ground-state phase was identified as $\mathcal{T}$ with "C1" Co-Fe and AFM-C spin orderings (Fig. 1) and a giant electric polarization of 165 $\mu C/cm^2$ (Supplemental Material, Fig. 3 [40]). The first metastable phase lies 55 meV/f.u. above the ground state and corresponds to a $\mathcal{R}$ structure presenting "C3" Co-Fe and AFM-G spin orderings (Fig. 1) and an electric polarization of 65 $\mu C/cm^2$ (Supplemental Material, Fig. 3 [40]). It is worth noting that the energies of the $\mathcal{M}$ and $\mathcal{R}$ phases are practically degenerate in the AFM-G case. On the other hand, the energies of the two studied orthorhombic phases are systematically larger than those of the other phases (Fig. 1 and Supplemental Material, Fig. 2 [40]). (Upon large pressures of ∼4 GPa one of the two considered orthorhombic phases becomes the ground state, Supplemental Material, Fig. 2 [40]; however, since here we are interested in phase transitions occurring at lower pressures, we will ignore those two phases hereafter.) By using analogous computational methods to ours, Diéguez and Íñiguez [46] concluded that the $BFCO_{0.5}$ ground state was a $\mathcal{R}$ phase with AFM-G spin ordering. The reason for the disagreement with our results lies in the fact that the DFT exchange-correlation functionals employed in both studies are different (i.e., PBE in the present study and PBEsol in [46]; Supplemental Material, Fig. 4 [40]).

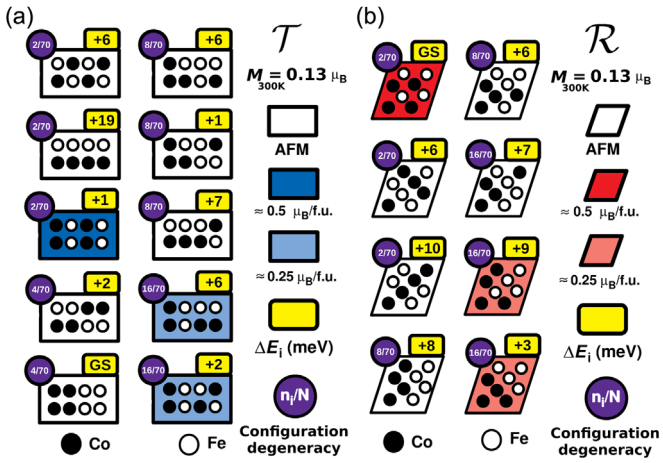

FIG. 2. First-principles determination of the magnetic properties of bulk $BFCO_{0.5}$ for phases (a) $\mathcal{T}$ and (b) $\mathcal{R}$. All possible atomic Co-Fe arrangements were generated for a $2 \times 2\sqrt{2} \times \sqrt{2}$ simulation cell containing 40 atoms, which were reduced by crystal symmetry operations to 10 $\mathcal{T}$ and 8 $\mathcal{R}$ representative configurations [48]. The magnetic moment, total energy, and relative degeneracy of each representative configuration are indicated. The room-temperature saturated magnetization estimated for each phase is $\approx 0.13\ \mu_B$ per formula unit. "GS" stands for ground state and $\Delta E_i \equiv E_i - E_{\mathrm{GS}}$.

Nevertheless, our zero-temperature PBE results appear to be more consistent with the recent observations by Azuma and co-workers, in which the stable phase of $BFCO_{0.5}$ has been experimentally identified as $\mathcal{T}$ [28,29], and also with the results of hybrid HSE06 calculations (Supplemental Material, Fig. 5 and Discussion I [40]).

To correctly describe the magnetic properties of the $\mathcal{T}$ and $\mathcal{R}$ phases at finite temperatures, we performed a systematic configurational analysis for a larger simulation cell containing 40 atoms (Fig. 2). The $\mathcal{T}$ and $\mathcal{R}$ configurations were initialized with AFM-C and AFM-G spin orderings, respectively, thus rendering zero net magnetizations. Upon full optimization, however, a considerable fraction of states exhibited a net magnetization of either 0.5 or 0.25 μ_B/f.u. (Fig. 2) due to a spin imbalance between the Co and Fe sublattices (Supplemental Material, Fig. 6 [40]). The $\mathcal{T}$ phase with the lowest energy displayed AFM-C spin ordering and zero net magnetization, while the $\mathcal{R}$ ground state was ferrimagnetic with a net magnetization of 0.50 μ_B/f.u. (Fig. 2). At equilibrium conditions, and considering only configurational effects, each configuration contributes to the total magnetization of the crystal as [48,49]

$$M(T) = \sum_{i}^{N_{\mathrm{conf}}} M_i \frac{\exp\left(-\Delta E_i / k_B T\right)}{Z_{\mathrm{conf}}}, \qquad (1)$$

where N_{conf} is the total number of configurations, M_i (E_i) is the zero-temperature magnetization (energy) of the ith configuration, $\Delta E_i \equiv E_i - E_0$, E_0 is the ground-state energy, k_B is the Boltzmann constant, and $Z_{\mathrm{conf}} \equiv \sum_i^{N_{\mathrm{conf}}} \exp\left(-\Delta E_i / k_B T\right)$ is the configurational partition function. By using Eq. (1) and the data reported in Fig. 2, we estimated that the saturated magnetization of both $\mathcal{T}$ and $\mathcal{R}$ phases amount to 0.13 μ_B/f.u. near room temperature (Supplemental Material, Fig. 7 [40]). In order to consider also the effects of thermal excitations on magnetic ordering, we performed a number of subsidiary Monte Carlo (MC) simulations for a spin Heisenberg model fitted to our DFT data [20,21,34,40,50]. Our MC simulations predict that the magnetic ferrimagnetic → paramagnetic transition temperature for the $\mathcal{T}$ and $\mathcal{R}$ phases are 325 ± 25 and 650 ± 25 K, respectively (Supplemental Material, Fig. 7 [40]). The large transition temperature difference between the $\mathcal{T}$ and $\mathcal{R}$ phases suggests the possibility of additional magnetic functionality near room temperature. We note that our theoretical results are consistent with a recent experimental work by Gao *et al.* in which robust ferrimagnetism has been reported for $BFCO_{0.5}$ thin films at room temperature [30].

Figure 3(a) shows the P–T phase diagram estimated for bulk $BFCO_{0.5}$ with first-principles methods and the QH approximation [34,43]. At low temperatures, a P-induced $\mathcal{T} \rightarrow \mathcal{R}$ phase transition occurs around 1 GPa. This transition renders a huge volume collapse of ∼10% ($\Delta V = V_{\mathcal{T}} - V_{\mathcal{R}} > 0$), which indicates a marked first-order character (Supplemental Material, Fig. 3 [40]). The corresponding P–T phase boundary, determined with the condition $\Delta G = G_{\mathcal{T}} - G_{\mathcal{R}} = 0$, where $G \equiv E + PV - TS$ represents the Gibbs free energy and S the entropy, exhibits a positive slope. Consequently, by the Clausius-Clapeyron

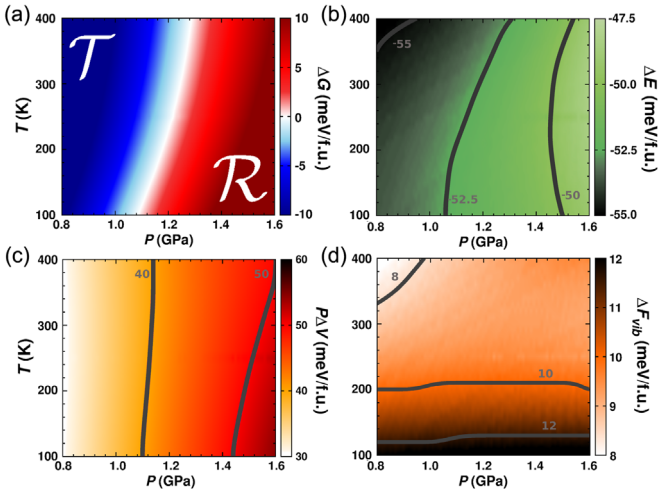

FIG. 3. Gibbs free-energy difference between the $\mathcal{T}$ and $\mathcal{R}$ phases of bulk $BiFe_{0.5}Co_{0.5}O_3$ and their contributions expressed as a function of temperature and pressure ($\Delta A \equiv A_{\mathcal{T}} - A_{\mathcal{R}}$). (a) Total Gibbs free-energy difference. (b) Static internal energy difference. (c) Enthalpy-related energy difference. (d) Vibrational Helmholtz free-energy difference. Thermodynamic states presenting equal ΔA values are joined by thick solid lines.

relation $\Delta S/\Delta V = \partial P/\partial T$, the entropy of the $\mathcal{T}$ phase should be larger than that of the $\mathcal{R}$ phase, namely, $\Delta S = S_{\mathcal{T}} - S_{\mathcal{R}} > 0$. Our QH free-energy calculations explicitly confirm this result since the value of the Helmholtz free-energy difference, $\Delta F = F_{\mathcal{T}} - F_{\mathcal{R}}$, decreases under increasing temperature [Fig. 3(d)] and $\Delta S \equiv -\partial \Delta F/\partial T$. It is noted that the only source of entropy considered in our calculations is vibrational, hence the subscript "vib" in Fig. 3(d); we assume that at low temperatures the magnetic and configurational entropies are small and very similar for the two phases (i.e., the $\{M_i\}$, $\{E_i\}$, and configurational degeneracy spectra calculated for $\mathcal{T}$ and $\mathcal{R}$ are much alike, Fig. 2 [48]), thus they hardly have any influence on ΔG.

The $BFCO_{0.5}$ phase diagram in Fig. 3(a) also shows an unusual T-induced $\mathcal{R} \rightarrow \mathcal{T}$ phase transition occurring at room temperature and a moderate hydrostatic pressure of 1.2 ± 0.2 GPa, for which the electric polarization of the bulk material increases by ~150% (Supplemental Material, Fig. 3 [40]). Such a T-induced phase transformation is mainly driven by entropy effects (i.e., term ΔF_{vib} in ΔG). This conclusion is straightforwardly deduced from Figs. 3(b)–3(d), since at fixed pressure the ΔE and $P\Delta V$ energy terms remain practically constant as a function of T [isovalue lines in Figs. 3(b) and 3(c) are roughly vertical], whereas ΔF_{vib} changes abruptly [isovalue lines in Fig. 3(d) are roughly horizontal]. It is worth noting that the disclosed T-induced $\mathcal{R} \rightarrow \mathcal{T}$ phase transition has neither been predicted nor observed previously for bulk $BiCoO_3$ or $BiFeO_3$ thin films. For instance, in bulk BCO, the P–T phase boundary involving the supertetragonal phase presents a negative slope [19], which implies a reduction in the stability of the $\mathcal{T}$ phase under increasing temperature and the typical electric polarization behavior $dp/dT < 0$ [20,21].

In view of the prominent role played by the lattice excitations on the anomalous T-induced stabilization of the $\mathcal{T}$ phase at room temperature, we performed a detailed analysis on the phonon modes and frequencies of $BFCO_{0.5}$ (Fig. 4). In particular, we estimated the projected density of vibrational states (PDOS) and Grüneisen parameter, defined as $\gamma_i \equiv -d \ln \omega_i / d \ln V$, for a large set of vibrational lattice frequencies $\{\omega_i\}$ (the same as employed for the calculation of accurate QH free energies). The PDOS of $BFCO_{0.5}$ generally is characterized by a low-ω nonpolar phonon region governed by Bi displacements ($0 < \omega \lesssim 4$ THz), followed by a medium-ω polar phonon interval dominated by transition-metal and oxygen ions ($4 \lesssim \omega \lesssim 10$ THz), and a high-ω nonpolar phonon region governed almost exclusively by oxygen vibrations ($\omega \gtrsim 10$ THz) (Fig. 4 and Supplemental Material, Fig. 8 [40]). Since here we are interested in phase transitions occurring near room temperature, only those phonon excitations belonging to the interval $0 < \omega \lesssim 6$ THz are relevant (i.e., $k_B T_{\text{room}} = 6.25$ THz and $\hbar\omega_i < k_B T_{\text{room}}$

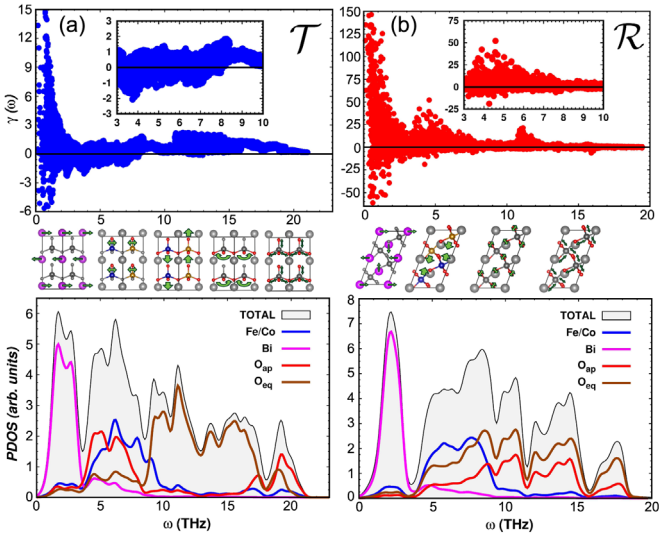

FIG. 4. Vibrational properties of the (a) $\mathcal{T}$ and (b) $\mathcal{R}$ phases of bulk $BiFe_{0.5}Co_{0.5}O_3$. The represented quantities are the Grüneisen parameter $\gamma(\omega)$ and the density of vibrational states along with the corresponding ionic contributions (PDOS). O_{ap} and O_{eq} stand for oxygen atoms in apical and equatorial positions, respectively. Some representative phonon eigenmodes are sketched with green arrows and they are ordered according to their vibrational frequency.

contribute the most to F_{vib} [51]). The number of Bi-dominated low-energy phonon modes is higher in the $\mathcal{R}$ phase than in the $\mathcal{T}$ phase (see PDOS peaks appearing at $\omega \approx 2$ THz in Fig. 4), hence the positive sign of the ΔF energy difference [Fig. 3(d)]. However, the number of vibrational states with frequencies $2 \lesssim \omega \lesssim 6$ THz is larger in the $\mathcal{T}$ phase than in the $\mathcal{R}$ phase (e.g., "bell-like" lattice modes involving concerted transition-metal and oxygen displacements are missing in the latter phase, Fig. 4) and, consequently, as the temperature is increased, ΔF gets reduced, leading to $\Delta S > 0$. Meanwhile, positive (negative) γ values indicate vibrational phonon frequencies that become "stiffer" ("softer") under pressure since the bulk modulus of $BFCO_{0.5}$ is positive (as we have explicitly checked). Consequently, based on the insets of Fig. 4, upon compression the number of phonon frequencies contained in the interval $2 \lesssim \omega \lesssim 6$ THz is further depleted in the $\mathcal{R}$ phase as compared to the $\mathcal{T}$ phase (that is, $-10 \lesssim \gamma_{\mathcal{R}} \lesssim +50$, while $-2 \lesssim \gamma_{\mathcal{T}} \lesssim +1$). This last outcome explains the fact that the $\mathcal{T}$ stability region expands in pressure as the temperature is increased, which leads to the positive slope of the $\mathcal{T}$–$\mathcal{R}$ phase boundary [Fig. 3(a)].

The unique entropy-driven stabilization of $\mathcal{T}$ $BFCO_{0.5}$ occurs at $P \sim 1$ GPa. For practical applications, it would be desirable that such transformation occurred at lower pressures. Our DFT calculations carried out for $BFCO_{0.25}$ indicate that the $\mathcal{T} \rightarrow \mathcal{R}$ critical pressure P_c can be reduced drastically by varying the composition of the solid solution. In particular, we estimate that P_c may be

reduced by a staggering 70% by increasing the Fe content from 50% up to 75% (Supplemental Material, Fig. 9 [40]). Interestingly, by repeating the same first-principles configurational analysis that was performed for $BFCO_{0.5}$, we found that both the bulk $BFCO_{0.25}$ $\mathcal{R}$ and $\mathcal{T}$ phases are also ferrimagnetic and exhibit a considerable saturated magnetization of 0.13 μ_B/f.u. near room temperature (Supplemental Material, Figs. 10 and 11 [40]). Moreover, the electric polarization of bulk $BFCO_{0.25}$ also changes by ~150% upon the $\mathcal{T} \rightarrow \mathcal{R}$ phase transition (Supplemental Material, Fig. 11 [40]). Therefore, we may conclude that the main characteristics of the $BFCO_{0.5}$ $\mathcal{R} \leftrightarrow \mathcal{T}$ phase transformation can be preserved and shifted down toward ambient conditions by adjusting the relative content of Co-Fe cations. It is worth mentioning that the experimental BFCO phase diagram determined by Azuma and co-workers as a function of temperature and composition appears to be consistent with our theoretical findings [28,29]. Finally, we analyzed the impact of likely nonergodic cation redistribution effects occurring during the $\mathcal{T} \leftrightarrow \mathcal{R}$ transformation on our main findings (Supplemental Material, Figs. 12 and 13 and Discussion II [40]). It was found that the general conclusions obtained when considering thermal equilibrium conditions are barely affected by the existence of nonergodic processes.

In conclusion, we predict that a ferrimagnetic $\mathcal{T}$ phase can be stabilized by means of T, P, and composition in bulk BFCO solid solutions near room temperature. The unusual temperature-induced $\mathcal{T}$ phase stabilization involves a colossal increase in the electric polarization of ~150% and a volume expansion of ~10% as referred to the corresponding low-T phase, which are promising features for nanoelectronics and energy conversion applications. In view of the low-cost and scalable chemical solution methods that are available for the synthesis of BFCO solid solutions [52], we expect that our theoretical work will stimulate new and exciting experimental research on $\mathcal{T}$ multiferroics.

Computational resources and technical assistance were provided by the Australian Government and the Government of Western Australia through the National Computational Infrastructure (NCI) and Magnus under the National Computational Merit Allocation Scheme and the Pawsey Supercomputing Centre. C. C. acknowledges support from the Spanish Ministry of Science, Innovation, and Universities under the "Ramón y Cajal" fellowship RYC2018-024947-I.

[1] L. Zhang *et al.*, Science **361**, 494 (2018).
[2] H. Yamada *et al.*, ACS Nano **7**, 5385 (2013).
[3] I. C. Infante *et al.*, Phys. Rev. Lett. **107**, 237601 (2011).
[4] X.-Y. Chen, L.-J. Chen, X.-B. Yang, Y.-J. Zhao, H.-C. Ding, and C.-G. Duan, J. Appl. Phys. **111**, 013901 (2012).
[5] C.-Y. Kuo *et al.*, Nat. Commun. **7**, 12712 (2016).
[6] J.-G. Park, M. D. Le, J. Jeong, and S. Lee, J. Phys. Condens. Matter **26**, 433202 (2014).
[7] J. T. Heron *et al.*, Nature (London) **516**, 370 (2014).
[8] J. Allibe, S. Fusil, K. Bouzehouane, C. Daumont, D. Sando, E. Jacquet, C. Deranlot, M. Bibes, and A. Barthélémy, Nano Lett. **12**, 1141 (2012).
[9] J. P. Domann and G. P. Carman, J. Appl. Phys. **121**, 044905 (2017).
[10] T. Nan *et al.*, Nat. Commun. **8**, 296 (2017).
[11] H. Yamamoto, T. Ogata, Y. Saki, and M. Azuma, Inorg. Chem. **58**, 2755 (2019).
[12] Z. Pan *et al.*, Chem. Mater. **31**, 1296 (2019).
[13] Ll. Mañosa and A. Planes, Adv. Mater. **29**, 1603607 (2017).
[14] C. Cazorla, Appl. Phys. Rev. **6**, 041316 (2019).
[15] J. Min, A. K. Sagotra, and C. Cazorla, Phys. Rev. Mater. **4**, 015403 (2020).
[16] A. A. Belik *et al.*, Chem. Mater. **18**, 798 (2006).
[17] J. Wang *et al.*, Science **299**, 1719 (2003).
[18] C. Menéndez, D. Chu, and C. Cazorla, npj Comput. Mater. **6**, 76 (2020).
[19] K. Oka *et al.*, J. Am. Chem. Soc. **132**, 9438 (2010).
[20] C. Cazorla, O. Diéguez, and J. Íñiguez, Sci. Adv. **3**, e1700288 (2017).
[21] C. Cazorla and J. Íñiguez, Phys. Rev. B **98**, 174105 (2018).
[22] Y. Heo, S. Hu, P. Sharma, K.-E. Kim, B.-K. Jang, C. Cazorla, C.-H. Yang, and J. Seidel, ACS Nano **11**, 2805 (2017).
[23] J. C. Wojdel and J. Íñiguez, Phys. Rev. Lett. **105**, 037208 (2010).
[24] G. J. MacDougall, H. M. Christen, W. Siemons, M. D. Biegalski, J. L. Zarestky, S. Liang, E. Dagotto, and S. E. Nagler, Phys. Rev. B **85**, 100406(R) (2012).
[25] C. R. Bowen, J. Taylor, E. LeBoulbar, D. Zabek, A. Chauhan, and R. Vaish, Energy Environ. Sci. **7**, 3836 (2014).
[26] M. Hoffmann, U. Schroeder, C. Künneth, A. Kersch, S. Starschich, U. Böttger, and T. Mikolajick, Nano Energy **18**, 154 (2015).
[27] T. Gottschall, A. Gràcia-Condal, M. Fries, A. Taubel, L. Pfeuffer, L. Mañosa, A. Planes, K. P. Skokov, and O. Gutfleisch, Nat. Mater. **17**, 929 (2018).
[28] M. Azuma, S. Niitaka, N. Hayashi, K. Oka, M. Takano, H. Funakubo, and Y. Shimakawa, Jpn. J. Appl. Phys. **47**, 7579 (2008).
[29] H. Hojo, K. Oka, K. Shimizu, H. Yamamoto, R. Kawabe, and M. Azuma, Adv. Mater. **30**, 1705665 (2018).
[30] B. Gao *et al.*, Phys. Rev. Mater. **2**, 084401 (2018).
[31] J. P. Perdew, K. Burke, and M. Ernzerhof, Phys. Rev. Lett. **77**, 3865 (1996).
[32] J. Heyd, G. E. Scuseria, and M. Ernzerhof, J. Chem. Phys. **118**, 8207 (2003).
[33] G. Kresse and J. Furthmüller, Phys. Rev. B **54**, 11169 (1996).
[34] C. Cazorla and J. Íñiguez, Phys. Rev. B **88**, 214430 (2013).
[35] P. E. Blöchl, Phys. Rev. B **50**, 17953 (1994).
[36] C. Cazorla and M. Stengel, Phys. Rev. B **92**, 214108 (2015).
[37] R. D. King-Smith and D. Vanderbilt, Phys. Rev. B **47**, 1651 (R) (1993).
[38] R. Resta, Rev. Mod. Phys. **66**, 899 (1994).

[39] L. Bellaiche and D. Vanderbilt, Phys. Rev. Lett. **83**, 1347 (1999).
[40] See Supplemental Material at http://link.aps.org/supplemental/10.1103/PhysRevLett.125.117601 for additional details on the structural, vibrational, magnetic, and ferroelectric properties of bulk $BiFe_{1-x}Co_xO_3$ solid solutions (cases $x = 0.5$ and 0.25); the Supplemental Material includes Refs. [41,42].
[41] J. P. Perdew, A. Ruzsinszky, G. I. Csonka, O. A. Vydrov, G. E. Scuseria, L. A. Constantin, X. Zhou, and K. Burke, Phys. Rev. Lett. **100**, 136406 (2008).
[42] K. T. Williams, L. K. Wagner, C. Cazorla, and T. Gould, arXiv:2005.03792.
[43] C. Cazorla and J. Boronat, Rev. Mod. Phys. **89**, 035003 (2017).
[44] G. Kresse, J. Furthmüller, and J. Hafner, Europhys. Lett. **32**, 729 (1995).
[45] D. Alfè, Comput. Phys. Commun. **180**, 2622 (2009).
[46] O. Diéguez and J. Íñiguez, Phys. Rev. Lett. **107**, 057601 (2011).
[47] S. Prosandeev, D. Wang, W. Ren, J. Íñiguez, and L. Bellaiche, Adv. Funct. Mater. **23**, 234 (2013).
[48] J. N. Shenoy, J. N. Hart, R. Grau-Crespo, N. L. Allan, and C. Cazorla, Adv. Theory Simul. **2**, 1800146 (2019).
[49] Y. Li-Juan, W. Ling-Zhi, and D. Shuai, Chin. Phys. B **24**, 127702 (2015).
[50] M. A. Sattar, S. A. Ahmad, F. Hussain, and C. Cazorla, J. Materiomics **5**, 404 (2019).
[51] C. Cazorla and T. Gould, Sci. Adv. **5**, eaau5832 (2019).
[52] P. Machado *et al.*, Chem. Mater. **31**, 947 (2019).